Available online at www.sciencedirect.com

Journal of Applied Research and Technology

Journal of Applied Research and Technology 14 (2016) 184–190

www.jart.ccadet.unam.mx

Original

Composite flywheel material design for high-speed energy storage

Michael A. Conteh, Emmanuel C. Nsofor *

Southern Illinois University, Carbondale, IL 62901, USA

Received 2 October 2015; accepted 12 April 2016
Available online 20 May 2016

Abstract

Lamina and laminate mechanical properties of materials suitable for flywheel high-speed energy storage were investigated. Low density, low modulus and high strength composite material properties were implemented for the constant stress portion of the flywheel while higher density, higher modulus and strength were implemented for the constant thickness portion of the flywheel. Design and stress analysis were used to determine the maximum energy densities and shape factors for the flywheel. Analytical studies along with the use of the CADEC-online software were used to evaluate the lamina and laminate properties. This study found that a hybrid composite of M46J/epoxy–T1000G/epoxy for the flywheel exhibits a higher energy density when compared to known existing flywheel hybrid composite materials such as boron/epoxy–graphite/epoxy. Results from this study will contribute to further development of the flywheel that has recently re-emerged as a promising application for energy storage due to significant improvements in composite materials and technology.
All Rights Reserved © 2016 Universidad Nacional Autónoma de México, Centro de Ciencias Aplicadas y Desarrollo Tecnológico. This is an open access item distributed under the Creative Commons CC License BY-NC-ND 4.0.

Keywords: Flywheel; Energy storage; High-speed; Composites; Energy-density

1. Introduction

Energy storage technologies are becoming practical solutions for situations where energy is required to be saved for use at a different time. Today, viable energy storage technologies include flywheels and batteries. The flywheel has recently re-emerged as a promising application for energy storage due to significant improvements in materials and technology. When compared to conventional energy storage systems, the flywheel has many advantages which include high power/energy density, much less environmental problems, availability of output energy directly in mechanical form and high efficiency. Composite materials flywheel allow for much higher density than conventional steel-based flywheels due to their lower density and potentially higher tensile strength.

One of the first studies which showed that composite materials with significantly large specific strength are well suited for flywheel energy storage applications was Rabenhorst (1971). Aspects of the report on comparison of flywheel material properties indicated that the use of 70% graphite whisker/epoxy material for the flywheel leads to a factor of 17.6 improvement over maraging steel that was considered to be the highest strength isotropic material for a constant stress flywheel rotor. DeTeresa and Groves (2001) examined the performance of commercial high-performance reinforcement fibers for application to flywheel power supplies and concluded that carbon fibers are preferred for highest performance. Dems and Turant (2009) presented methods for the design of reinforced composite flywheels for maximum kinetic energy while Tzeng, Emerson, and Moy (2006) studied elastic and viscoelastic behavior of composite flywheels and proposed methodology, material characterization and test matrices for the design in order to achieve maximum performance. Clerk (1964) pointed out that a major requirement is the need to significantly increase the energy density and Janse, Petrus, Groenwold, and Wood (2013) studied some composite flywheel rotor design methods and proposed a formulation for improvement toward achieving high energy density.

Wen and Jiang (2012) reported on maximizing the energy storage capacity of a hybrid composite multi-ring flywheel. Results show that the composed rings of the hybrid flywheel

* Corresponding author.
E-mail address: nsofor@siu.edu (E.C. Nsofor).
Peer Review under the responsibility of Universidad Nacional Autónoma de México.

http://dx.doi.org/10.1016/j.jart.2016.04.005
1665-6423/All Rights Reserved © 2016 Universidad Nacional Autónoma de México, Centro de Ciencias Aplicadas y Desarrollo Tecnológico. This is an open access item distributed under the Creative Commons CC License BY-NC-ND 4.0.

Nomenclature

A, B, D	extension, extension-bending, bending stiffnesses respectively
E	Young's modulus
F	lamina strength
K	shape factor
KE	kinetic energy
N	force resultant; number of lamina
M	moment resultant
R	laminate strength
e	energy density
h	axial thickness of flywheel
k	integration constant; curvature
m	mass
n	number of sequence repetition
r	radius
u	displacement

Greek symbols

ε	strain
θ	LAMINA lay-up
ν	Poisson's ratio
σ	stress
ρ	density
ω	angular velocity

Subscripts

1	fiber direction
a, b	disk and rim respectively; outer position of disk and rim respectively
o	center of flywheel
r, θ	cylindrical coordinate directions
t, c	tensile and compressive
x, y, z	Cartesian coordinates directions

Superscripts

0	In-plane

rotor can nearly reach the limits of strength in both radial and circumferential directions. Ha, Kim, Nasir, and Han (2012) studied different rim design cases of hybrid composite flywheel rotor based on strength ratio optimization. The rotor was composed of four composite rims made of carbon-glass/epoxy with hoop wound reinforcements of varying volume fractions. Alexandrova and Vila Real (2009) designed composite flywheel based on the model of annular rotating disk with stress-free boundary condition while thin rim or multi-trim flywheel was reported by Post and Post (1973) where individual thin rings basically in pure uniaxial stress circumferentially were made to spin about a common axis. Wang, He, Zhao, and Li (2012) studied a multilayer rim carbon fiber/glass fiber, composite flywheel for ultimate strength requirement. Results show that selecting the layer thickness and hybrid ratio of carbon fiber to glass fiber can reduce radial strength requirement of the rim material.

Studies (Bolund, Bernhoff, & Leijon, 2007; Chang & Hirschfeld, 1978; Genta, 1985; Kirk, 1977) have found that possible flywheel shapes for energy storage include the constant stress disk, conical disk, constant thickness (pierced and unpierced) disk, disk with rim and thin rim. Metwalli, Shawki, and Sharobeam (1983) designed configurations that maximize the energy density of variable material flywheels and proposed an optimum design of a constant stress flywheel whose material density varies radially. One of the conclusions reached in the study is that a multi-element alloy flywheel will provide a higher inertia per unit mass than a flywheel made of one element with a higher specific strength. Georgian (1989) reported on the optimum design of composite flywheel consisting of inner disk of low density, high strength and low modulus of elasticity composite material and an outer disk of constant thickness with high density, high strength and high modulus of elasticity. The results show that maximum energy density was achieved using a combination boron/epoxy for the rim and high strength graphite/epoxy for the constant stress portion of the flywheel leading to the conclusion that in order to obtain high energy densities, a search for a higher strength and lower density composite for the disk is required. This present study investigated composite materials with low densities, low modulus and high strength for the constant stress portion and a higher density, higher modulus and strength for the constant thickness portion. Analytical studies along with the use of the CADEC-online software were used to evaluate the lamina and laminate properties.

2. Flywheel stress analysis

Figure 1 shows the views of the flywheel used in the study. It is a constant stress disk and a constant thickness rim flywheel with an angular velocity of ω rad/s. The sectioned annular element at a radius, r, is in equilibrium under the action of the forces shown.

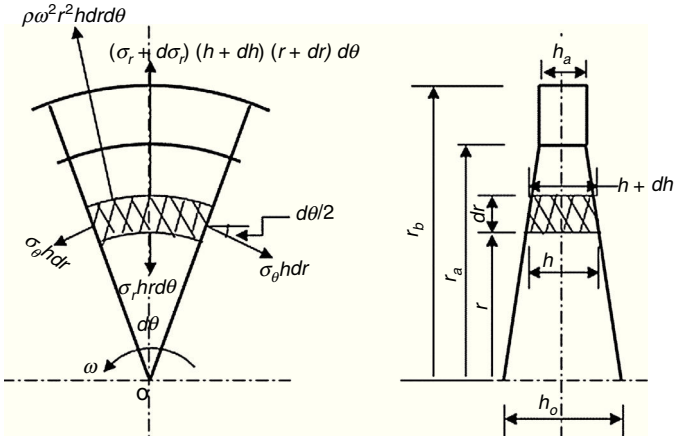

Fig. 1. Constant stress disk and constant thickness rim flywheel.

The equilibrium and compatibility equations can be shown respectively to be (Stodola, 1945):

$$h\sigma_r + r\sigma_r\frac{dh}{dr} + hr\frac{d\sigma_r}{dr} - h\sigma_\theta + \rho hr^2\omega^2 = 0 \tag{1}$$

$$\frac{d\sigma_\theta}{dr} - \nu\frac{d\sigma_r}{dr} = (1+\nu)\frac{(\sigma_r - \sigma_\theta)}{r} \tag{2}$$

The strain–stress relations of an isotropic material are given as:

$$\begin{aligned}\sigma_r &= \frac{E}{1-\nu^2}[\varepsilon_r + \nu\varepsilon_\theta]\\ \sigma_\theta &= \frac{E}{1-\nu^2}[\nu\varepsilon_r + \varepsilon_\theta]\end{aligned} \tag{3}$$

and the strain–displacement relations are given as:

$$\varepsilon_r = \frac{du_r}{dr} \quad \text{and} \quad \varepsilon_\theta = \frac{u_r}{r} \tag{4}$$

Substituting (4) in (3) and then in (1) simplifies to give

$$\frac{d^2u_r}{dr^2} + \left[\frac{1}{h}\frac{dh}{dr} + \frac{1}{r}\right]\frac{du_r}{dr} + \left[\frac{\nu}{hr}\frac{dh}{dr} - \frac{1}{r^2}\right]u_r + Ar = 0 \tag{5}$$

where

$$A = \frac{(1-\nu^2)\rho\omega^2}{E}$$

Consideration of the constant stress disk makes (1) to become

$$\frac{dh}{h} = -\frac{\rho\omega^2}{\sigma}rdr \tag{6}$$

Integrating (6) and noting that at $r = r_a$, $h = h_a$ gives

$$h = h_a e^{B[1-(r/r_a)^2]} \tag{7}$$

where

$$B = \frac{\rho\omega^2 r_a^2}{2\sigma} \tag{8}$$

It is noted that for the rim, $h = h_a =$ constant. Substitution of this in (5) gives

$$\frac{d^2u_r}{dr^2} + \frac{1}{r}\frac{du_r}{dr} - \frac{1}{r^2}u_r + Ar = 0$$

whose solution can be shown to be

$$u_r = -\frac{Ar^3}{8} + k_1 r + \frac{k_2}{r} \tag{9}$$

where k_1 and k_2 are integration constants.

Using the expression for u_r in (4) and the relations in (3) gives

$$\sigma_r = \frac{E}{1-\nu^2}\left[-(3+\nu)\frac{Ar^2}{8} + (1+\nu)k_1 - (1-\nu)\frac{k_2}{r^2}\right] \tag{10}$$

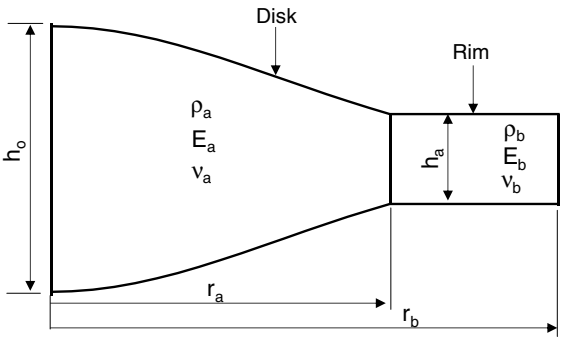

Fig. 2. Profile of proposed flywheel.

$$\sigma_\theta = \frac{E}{1-\nu^2}\left[-(3\nu+1)\frac{Ar^2}{8} + (1+\nu)k_1 + (1-\nu)\frac{k_2}{r^2}\right] \tag{11}$$

Georgian (1989) showed that the constant stress portion of the flywheel becomes bulgy for large values of $\ln(h_o/h_a)$. Thus, the center cannot carry its share of the rim load. Hence the limit of $\ln(h_o/h_a)$ for maximum energy density is approximately equal to 2. Figure 2 shows the profile of the constant stress disk flywheel used in this study. Based on the results of previous studies, the disk and rim are made of different composite materials with indicated elastic properties.

The stress distribution in the disk portion is given as

$$\sigma = \sigma_r = \sigma_\theta = \frac{\rho_a\omega^2 r_a^2}{2\ln(h_o/h_a)} \tag{12}$$

while the stress distribution in the rim is given as:

$$\sigma_r = \frac{E_b}{1-\nu_b^2}\left[-(3+\nu_b)\frac{Ar^2}{8} + (1+\nu_b)k_1 - (1-\nu_b)\frac{k_2}{r^2}\right] \tag{13}$$

$$\sigma_\theta = \frac{E_b}{1-\nu_b^2}\left[-(3\nu_b+1)\frac{Ar^2}{8} + (1+\nu_b)k_1 + (1-\nu_b)\frac{k_2}{r^2}\right] \tag{14}$$

where

$$A = \frac{(1-\nu_b^2)\rho_b\omega^2}{E_b}$$

The integration constants, k_1 and k_2 are obtained using the following boundary condition at the interface between the disk and rim, that is, at $r = r_a$.

$$\sigma_r(\text{disk}) = \sigma_r(\text{rim})$$

$$\varepsilon_\theta(\text{disk}) = \varepsilon_\theta(\text{rim})$$

Using the above boundary conditions, it can be shown that:

$$k_1 = \frac{(1-\nu_b)\rho_b\omega^2 r_b^2}{8E_b}\left[(3+\nu_b) + (1-\nu_b)\left\{\frac{2(\rho_a/\rho_b)}{\ln(h_o/h_a)}\left[\frac{E_b}{E_a}\frac{(1-\nu_a)}{(1-\nu_b)} - 1\right] - 1\right\}\left(\frac{r_a}{r_b}\right)^4\right] \tag{15}$$

and

$$k_2 = \frac{(1-\nu_b^2)\rho_b\omega^2}{8E_b}\left\{\frac{2(\rho_a/\rho_b)}{\ln(h_o/h_a)}\left[\frac{E_b}{E_a}\frac{(1-\nu_a)}{(1-\nu_b)} - 1\right] - 1\right\}r_a^4 \tag{16}$$

Eq. (17) gives the radii ratio (r_a/r_b). It is a ratio that gives the optimum radial dimensions of the flywheel.

$$\left(\frac{r_a}{r_b}\right)^4 - \left\{1 + \frac{(3+\nu_b) + 4(\rho_a/\rho_b)/\ln(h_o/h_a)}{\left[((2(\rho_a/\rho_b))/(\ln(h_o/h_a)))((E_b/E_a)(1-\nu_a) - (1-\nu_b)) - (1-\nu_b)\right]}\right\}\left(\frac{r_a}{r_b}\right)^2 + \frac{1}{\left[((2(\rho_a/\rho_b))/(\ln(h_o/h_a)))((E_b/E_a)(1-\nu_a) - (1-\nu_b)) - (1-\nu_b)\right]} = 0 \tag{17}$$

These dimensions satisfy the boundary conditions.

It should be noted that the stress analyses is for a flywheel with different materials for the constant stress portion and constant thickness rim taking into consideration the differences in the Poisson's ratios of the materials.

3. Energy density of the flywheel

Useful parameters for assessing flywheel systems include the energy density of the rotor and its associated shape factor, K. It can be shown that the energy density of the rotor at burst speed is dependent only on the flywheel design and on the characteristics of the material. As shown in Genta (1985) and other studies, the energy density is given as:

$$e = \frac{\mathrm{KE}}{m} = K\frac{\sigma}{\rho} \tag{18}$$

where e is the energy density, KE is the kinetic energy of the flywheel and m is the mass of the flywheel. σ and ρ are the tensile strength and density of the rotor material respectively.

The mass and mass moment of inertia can be shown to be respectively as

$$m = \rho_a \pi h_a r_a^2 \left[\frac{(e^B - 1)}{B} + \frac{\rho_b}{\rho_a}\left(\left(\frac{r_b}{r_a}\right)^2 - 1\right)\right] \tag{19}$$

$$I = \rho_a \pi h_a r_a^4 \left\{\frac{(-B + e^B - 1)}{B^2} + \frac{\rho_b}{2\rho_a}\left[\left(\frac{r_b}{r_a}\right)^4 - 1\right]\right\} \tag{20}$$

From (18), (19) and (20) it can be shown that the shape factor of the disk is given by:

$$K = \frac{(-B + e^B - 1) + (B^2/2)(\rho_b/\rho_a)[(r_b/r_a)^4 - 1]}{(e^B - 1) + B(\rho_b/\rho_a)[(r_b/r_a)^2 - 1]} \tag{21}$$

where B is defined as

$$B = \ln\left(\frac{h_o}{h_a}\right)$$

4. Composite material properties

The above analyses are for isotropic materials. Though the bending behavior of a quasi-isotropic laminate is not quite the same as an isotropic plate, a properly designed symmetric quasi-isotropic laminate can behave like an isotropic plate. The flywheel material for this study is assumed to be properly designed, symmetric and quasi-isotropic.

The classic plate theory is used in the analysis of laminates. It relates the force (N) and moment (M) resultants to the in-plain strains (ε^0) and curvatures (κ). This can be expressed as

$$\begin{bmatrix} N \\ M \end{bmatrix} = \begin{bmatrix} A & B \\ B & D \end{bmatrix} \begin{bmatrix} \varepsilon^0 \\ \kappa \end{bmatrix} \tag{22}$$

where the [ABD] matrix is obtained from the lamina properties. Many micromechanics models have been used to predict the properties of a composite lamina. As stated by Barbero (2011), the periodic microstructure micromechanics produces accurate predictions for all the moduli of a unidirectional lamina. This was used in the computation of the lamina properties.

In a symmetric quasi-isotropic laminate the bending-extension stiffness matrix [B] are zero. According to Akkerman (2001), the in-plane stiffnesses are independent of the composite orientation. The general lamina layup in a quasi-isotropic laminate is given (Barbero, 2011; Akkerman, 2001) as

$$\theta_k = \frac{n\pi}{N} + \theta_o \tag{23}$$

where k is the lamina number, N is the number of laminates ($N \geq 3$), and θ_o is an arbitrary reference angle. The practical quasi-isotropic laminate layups are $[0/\pm 60]_{\mathrm{nS}}$ and $[0/\pm 45/90]_{\mathrm{nS}}$, n being the number of sequence repetition. In terms of the extensional stiffness matrix, the laminate in-plane moduli are given (Barbero, 2011) as

$$\begin{aligned} E_x &= \frac{A_{11}A_{22} - A_{12}^2}{tA_{22}} \\ E_y &= \frac{A_{11}A_{22} - A_{12}^2}{tA_{11}} \\ G_{xy} &= \frac{A_{66}}{t} \\ \nu_{xy} &= \frac{A_{12}}{A_{22}} \end{aligned} \tag{24}$$

while the laminate strength, using the maximum stress criterion, is given as:

$$R = \left\{\frac{F_{1t}}{\sigma_1}\right\} + \left\{\frac{-F_{1c}}{\sigma_1}\right\} \tag{25}$$

A computer aided design environment for composite software (CADEC, 2011), developed by Barbero and available online, was used to evaluate the lamina and quasi-isotropic laminate elastic properties, using the periodic microstructure micromechanics for the lamina properties.

Table 1
Fiber and matrix properties.

	Fiber–polyacrylonitrile (PAN) (Toray, 2008)				Matrix (Ashland, 2015)
	T1000G	M35J	M46J	T-650/35	Epoxy (470-36S)
Density, ρ [g/cm^3]	1.8	1.75	1.84	1.77	1.150
Longitudinal modulus, E [GPa]	294	343	436	255	3.6
Poisson's ratio	0.2	0.2	0.2	0.2	0.38
Longitudinal tensile strength, F_t [MPa]	6370	4700	4210	4280	90

Table 2
Evaluated lamina properties with a volume fraction of 0.7.

	M35J/epoxy	M46J/epoxy	T1000G/epoxy	T650-35/epoxy
Density [g/cm^3]	1.57	1.633	1.605	1.584
Longitudinal modulus, E_1 [GPa]	241.2	306.3	206.9	179.6
Transverse modulus, E_2 [GPa]	18.16	18.42	17.96	17.75
In-plane Poisson's ratio, ν_{12}	0.246	0.2459	0.246	0.2461
Intralamina Poisson's ratio, ν_{23}	0.5357	0.5375	0.5344	0.533
In-plane shear modulus, G_{12} [GPa]	7.195	7.271	7.137	7.075
Intralamina shear modulus, G_{23} [GPa]	5.912	5.99	5.851	5.789
Longitudinal tensile strength, F_{1t} [MPa]	3305	2957	4482	3014
Longitudinal compressive strength, F_{1c} [MPa]	1528	1533	1523	1518
Transverse tensile strength, $F_{2t} = F_{2c}$ [MPa]	77.83	77.8	77.85	77.87
Intralamina shear strength, F_4 [MPa]	28.27	28.26	28.28	28.29
In-plane shear strength, F_6 [MPa]	77.81	77.79	77.83	77.85

Table 3
Evaluated quasi-isotropic laminate $[0/\pm 45/90]_S$, properties.

	M35J/Epoxy	M46J/Epoxy	T1000G/epoxy	T650-35/epoxy
Density [g/cm^3]	1.57	1.633	1.605	1.584
Longitudinal modulus, E_1 [GPa]	92.21	114.1	80.66	71.44
Transverse modulus, E_2 [GPa]	92.21	114.1	80.66	71.44
Shear modulus, G_{xy} [GPa]	35.04	43.23	30.71	27.25
Poisson's ratio, ν_{xy}	0.3157	0.319	0.3132	0.3107
Ultimate strength, F_t [MPa]	6323.75	5658.75	8577.50	5768.13

Table 4
Compared results of analyses.

Constant thickness material / Constant stress material		(r_a/r_b)		Shape factor (K)		Energy density (kJ/kg)	
Boron/epoxy / Graphite/epoxy	(High strength)	0.8354	**0.8357**	0.9467	**0.9462**	97.723	**97.673**
Boron/epoxy / Graphite/epoxy	(High modulus)	0.8387	**0.8380**	0.9395	**0.9409**	58.592	**58.683**

5. Results and discussion

Tables 1–3 show properties of the fiber and matrix, lamina and laminates respectively for volume fraction of 0.7 and lamina thickness of 1.6 mm. The laminate was designed with a 10% coefficient of variance for 95% reliability with respect to the first ply failure (FPF) using a reference load of 1000 N/mm.

For validation purposes, the results from this study were compared to those from Georgian (1989) using $\ln(h_o/h_a) = 2$, $r_b = 0.24$ m, $h_a = 0.02$ m and the quasi-isotropic composites material properties.

The bolded results in Table 4 are from this study. As can be seen the two analyses are in close agreement.

As stated in Georgian (1989) conclusion, in order to obtain high energy density a search for a higher strength, lower modulus and lower density for the constant stress portion is required. In his study boron/epoxy–graphite/epoxy composites combination gave the highest energy density. Hence, the materials being investigated were compared to boron/epoxy–graphite/epoxy. Table 5 shows a combination of composites from Table 3 and the high strength boron/epoxy–graphite/epoxy. A factor of safety of 3 was used for the constant stress portion (disk) of the flywheel. As seen from the listed energy densities,

Table 5
Different material combination for disk and rim of flywheel.

Constant thickness material / Constant stress material	Shape factor (K)	Energy density (KJ/kg)
Boron/epoxy / Graphite/epoxy	0.9467	97.723
M46J/epoxy / M35J/epoxy	0.9554	1282.8
M46J/epoxy / T1000G/epoxy	0.9647	1718.5
M46J/epoxy / T650-35/epoxy	0.9708	1178.3

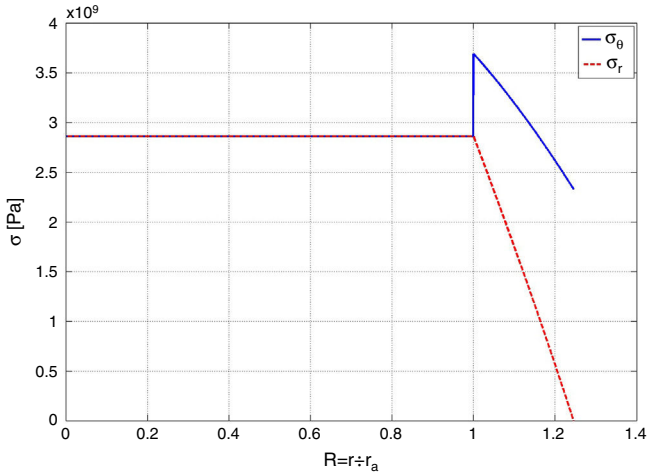

Fig. 3. Flywheel stress distribution for M46J/epoxy–T1000G/epoxy combination.

the combination of M46J/epoxy and T1000G/epoxy gives the maximum energy density. It is about 18 times more than the boron/epoxy–graphite/epoxy. This is due to the current high modulus and high strength carbon fibers.

Figure 3 shows the stress distribution of the flywheel for M46J/epoxy–T1000G/epoxy combination. The stress in the disk (constant stress portion) is 2859 MPa. The tangential stress in the rim (the constant thickness portion) has a maximum value of about 3689 MPa.

Previous published results have shown that in order to obtain higher energy densities, a search for a higher strength and lower density composite for the constant stress portion is required. This is clearly shown in this report. Properties of several composite materials suitable for flywheel energy storage were investigated. Design and stress analysis were used to determine for each material, the maximum energy densities and shape factor of the flywheel. The materials identified based on the results from this study outperformed the boron/epoxy–graphite/epoxy combination.

6. Conclusion

Previous research results have shown that in order to obtain higher flywheel energy densities, a search for a higher strength and lower density composite for the constant stress portion is required. Elaboration on this was done in this study. Properties of several composite materials suitable for flywheel energy storage were investigated. Design and stress analysis were used to determine the maximum energy density and shape factor for the flywheel. The materials identified for this, based on the results from this study demonstrated outperformance compared to the boron/epoxy–graphite/epoxy combination. Results from this study will contribute to aiding further development of the flywheel that has recently re-emerged as a promising application for energy storage due to significant improvements in composite materials and technology.

Conflict of interest

The authors have no conflicts of interest to declare.

References

Akkerman, R. (2001). On the properties of quasi-isotropic laminates. *Composites Part B – Engineering*, *33*(2), 133–140. http://dx.doi.org/10.1016/S1359-8368(02)00002-1

Alexandrova, N. N., & Vila Real, P. M. M. (2009). Preliminary design of a composite material flywheel. *Material Science Forum*, *623*, 21–35.

Ashland (2015). Available from www.ashland.com. Retrieved 17.10.13.

Barbero, E. J. (2011). *Introduction to composite material design*. New York, USA: Taylor & Francis Group.

Bolund, B., Bernhoff, H., & Leijon, M. (2007). Flywheel energy and power storage systems. *Renewable & Sustainable Energy Reviews*, *11*(2), 235–258. http://dx.doi.org/10.1016/j.rser.2005.01.004

CADEC (2011) Available at http://en.cadec-online.com. Accessed January 2015.

Chang, G. C., & Hirschfeld, F. (1978). For the latest in energy storage, try the flywheel. *Mechanical Engineering*, *100*(2), 38–45.

Clerk, R. C. (1964). *The utilization of flywheel energy*. pp. 508–543. (72) SAE International Summer Meeting.

Dems, K., & Turant, J. (2009). Two approaches to the optimal design of composite flywheels. *Engineering Optimization*, *41*(4), 351–363. http://dx.doi.org/10.1080/03052150802506521

DeTeresa, S. J., & Groves, S. E. (2001). *Properties of fiber composites for advanced flywheel energy storage devices*. pp. 1643–1656. *A Materials and Processes Odyssey, Books 1 and 2* (vol. 46)

Genta, G. (1985). *Kinetic energy storage: Theory and practice of advanced flywheel systems*. pp. 80–83. London: Butterworth & Co. Ltd.

Georgian, J. C. (1989). Optimum design of variable composite flywheel. *Journal of Composite Materials*, *23*(1), 2–10.

Ha, S. K., Kim, S. J., Nasir, S. U., & Han, S. C. (2012). Design optimization and fabrication of a hybrid composite flywheel rotor. *Composite Structures*, *94*(11), 3290–3299. http://dx.doi.org/10.1016/j.compstruct.2012.04.015

Janse, V. R., Petrus, J., Groenwold, A. A., & Wood, D. W. (2013). Optimization of cylindrical composite flywheel rotors for energy storage. *Structural and Multidisciplinary Optimization*, *47*(1), 135–147.

Kirk, J. A. (1977). Flywheel energy-storage 1: Basic concepts. *International Journal of Mechanical Sciences*, *19*(4), 223–231. http://dx.doi.org/10.1016/0020-7403(77)90064-9

Metwalli, S. M., Shawki, G. S. A., & Sharobeam, M. H. (1983). Optimum design of variable-material flywheels. *Journal of Mechanisms Transmissions and Automation in Design – Transactions of the ASME*, *105*(2), 249–253.

Post, R. F., & Post, S. F. (1973). Flywheels. *Scientific American*, *229*, 17–23.

Rabenhorst, D. W. (1971). *Potential applications for the superflywheel*. pp. 1118–1125. Proceedings of the 6th Intersociety Energy Conversion Engineering Conference.

Stodola, A. (1945). *Steam and gas turbines: With a supplement on the prospects of the thermal prime mover*. pp. 372–380. New York, USA: Peter Smith.

Toray Carbon Fibers America, Inc. (2008). Available from www.toraycfa.com/product.html. Retrieved 17.10.13.

Tzeng, J., Emerson, R., & Moy, P. (2006). Composite flywheels for energy storage. *Composite Science and Technology*, *66*(14), 2520–2527.

Wen, S., & Jiang, S. (2012). Optimal design of hybrid composite multi-ring flywheel rotor based on displacement method. *Composite Science and Technology*, *72*(9), 982–988.

Wang, W., He, L., Zhao, X. F., & Li, G. X. (2012). Design of hybrid composite multilayer rim of high speed energy storage flywheels. *Advances in Materials Processing X*, *500*, 603–607. http://dx.doi.org/10.4028/www.scientific.net/AMR.500.603